

RF Pulse Optimization for Bloch-Siegert B_1^+ Mapping

M. M. Khalighi¹, B. K. Rutt², M. Saranathan², and A. B. Kerr³

¹Global Applied Science Laboratory, GE Healthcare, Menlo Park, CA, United States, ²Department of Radiology, Stanford University, Stanford, CA, United States, ³Department of Electrical Engineering, Stanford University, Stanford, CA, United States

Purpose: Bloch-Siegert (BS) B_1^+ mapping is an accurate and efficient method of B_1^+ mapping [1] with the significant advantage of being largely insensitive to tissue properties such as T_1 and T_2 . However, it suffers from long TE and high RF deposition (SAR) due to the long off-resonant RF pulse (BS pulse) used to create the measured BS shift in resonant frequency. The BS pulse has to have a frequency response that limits on-resonant excitation, yet it also has to create enough Bloch-Siegert phase shift for adequate BS B_1^+ map quality. Thus we sought to optimize the design of short BS pulses to be as close as possible to the water resonance frequency for maximum B_1^+ sensitivity while keeping the unwanted on-resonant excitation below a threshold.

Methods: A typical BS pulse is a large tip pulse ($> 1200^\circ$ if it were applied on resonance), however by virtue of being sufficiently off-resonant, the effective axis of rotation is nearly parallel to the longitudinal axis for resonant spins. As there is minimal perturbation to the longitudinal magnetization we can assume that the small-tip approximation [2] or simple Fourier analysis holds within the resonant band. Accordingly, we solve the following quadratic programming problem to design a low-pass filter that maximizes power:

$$\text{Minimize } -\frac{1}{2} \mathbf{x}^T \mathbf{I} \mathbf{x}, \text{ such that } |\mathbf{W}\mathbf{x}| < \delta, 0 < x(n) < 2\pi\gamma\Delta t B_{1,\max}, n = 1 \dots N$$

Where $x(n) = 2\pi\gamma\Delta t B_1(n)$ are the N scaled samples of the fixed-duration RF pulse, \mathbf{I} is the identity matrix, \mathbf{W} is a DFT matrix evaluating the stopband performance of the pulse, δ is the stopband ripple, $B_{1,\max}$ is the peak B_1 expected to be measured, and Δt is the duration of each RF sample. The minimization problem is solved using the quadratic programming solver provided by Matlab (The Mathworks, Natick, USA). As the problem is not strictly convex, local minima are avoided by seeding the program with a Fermi [1] window as an initial solution. This problem is solved for stopband frequency edges set from 1-4kHz. For each solution, a Bloch simulation is performed to calculate the actual stopband edge, the pulse modulated off-resonance and then a further Bloch simulation performed to determine which pulse provides the maximum Bloch-Siegert phase shift that would be accrued during a B_1^+ mapping experiment. Fig. 1 shows the 4-ms “Quad” pulse that was designed to limit excitation over a range of ± 600 Hz to less than 1% when modulated 1.94kHz off resonance, assuming a peak $B_{1,\max}$ of 20 μT . Fig. 2 shows the Bloch-Siegert phase shift as a function of B_1 and B_0 for both the Quad and Fermi pulses. The Bloch-simulated phase-shift dependence on B_1 and B_0 is tabulated in a 2D look-up table, from which B_1 maps are calculated given the measured BS phase shift and an acquired B_0 map. To minimize the on-resonant excitation effects of the BS pulse, crushers were added before and after BS pulse and the BS pulse was chopped every other phase encode (i.e. BS phase offset π radians with respect to excitation).

Results: The 4-ms Quad ($\Delta\omega_{BS}=1.94\text{kHz}$), and 6-ms Fermi ($\Delta\omega_{BS}=4\text{kHz}$) pulses are compared as BS pulses for B_1^+ mapping in a modified conventional gradient echo sequence (Fig. 3) [1] on a 7T scanner (GE Healthcare, Waukesha). Phantom studies were acquired using the following parameters: TR=50 ms, flip angle=40 deg, FOV=24 cm, thickness = 5 mm and 64×64 matrix. TE for the Quad pulse was 7.1 ms and for the Fermi pulse was 9.1 ms. The B_1^+ mapping sequence was repeated 20 times for each pulse and mean B_1^+ and angle-to-noise ratio (ANR) maps were computed, shown in Fig. 4-5. The nominally symmetric off-resonant pulses ($\pm\Delta\omega_{BS}$) were then both shifted up or down by 600 Hz to simulate B_0 off resonance effects. Fig. 3 shows all 3 maps (+600 Hz, 0Hz and -600 Hz offset) for both Fermi and Quad BS pulses, along with the difference map. The two off-resonance pulses were also compared on a volunteer with the same sequence with the exception of a longer TR=150 ms. Fig. 6 shows the comparison between Quad and Fermi off-resonant pulses in an axial plane of volunteer brain. The difference between the B_1^+ maps by these two pulses is less than 10% everywhere and in the areas with higher SNR is less than 2%.

Discussion: The comparison between Quad and Fermi off resonance pulses on phantom and head (Figs 3-6) show that the two pulses create high-quality comparable B_1^+ maps. Figure 3 shows that the LUT processing accurately compensates for B_0 inhomogeneity even in the presence of 600 Hz B_0 offsets. Figure 4 shows the agreement between B_1^+ maps is on the order of 1%, while Fig. 5 illustrates the improved ANR offered with the Quad pulse. Furthermore, the Quad pulse benefits from 35% less SAR and 2 ms shorter echo time, which is helpful at high field with the increased SAR and B_0 inhomogeneity. The B_0 map acquisition is typically not an additional burden in our case as this is already required for other quantitative studies.

References: [1] Sacolick et al., MRM 63:1315-1322, 2010. [2] Pauly et al., JMR 81:43-56, 1989.

Acknowledgement: Research support from GE Healthcare, NIH R01 EB008108, NIH R01 EB005307.

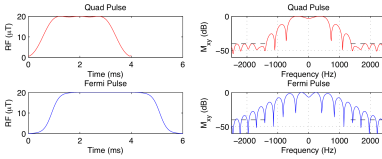


Fig. 1) Frequency response of BS pulses. Dashed line shows 1% excitation stopband over ± 600 Hz when offset 1.94kHz.

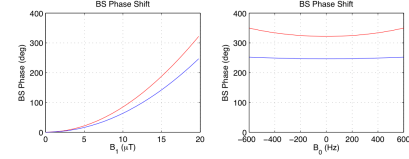


Fig. 2) BS phase dependence on $B_{1,\max}$ ($B_0=0\text{Hz}$), and B_0 ($B_{1,\max}=20\mu\text{T}$) for Quad (red) & Fermi (blue) pulses.

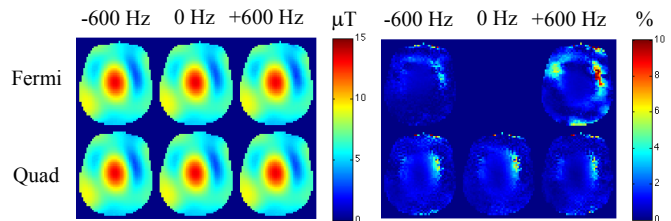


Fig. 3) BS B_1^+ mapping at different B_0 values.

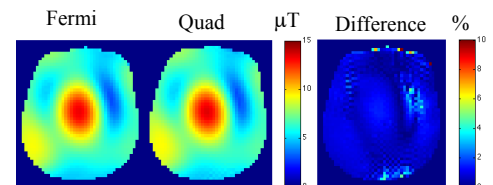


Fig. 4) Average of B_1^+ map with Fermi & Quad pulses

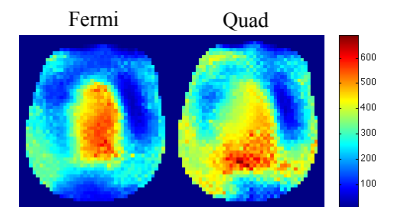


Fig. 5) ANR of B_1^+ with Fermi & Quad pulses

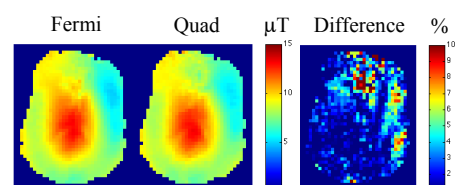


Fig. 6) Axial B_1^+ of brain with Fermi & Quad pulses